MATERIALS CHARACTERIZATION 68 (2012) 49–57

Available online at www.sciencedirect.com

SciVerse ScienceDirect

www.elsevier.com/locate/matchar

Microstructural evolution during solution treatment of Co–Cr–Mo–C biocompatible alloys

J.V. Giacchi[a,b,*], O. Fornaro[a,b], H. Palacio[a,c]

[a]IFIMAT, Instituto de Física de Materiales Tandil, Facultad de Ciencias Exactas, Universidad Nacional del Centro de la Provincia de Buenos Aires, Pinto 399, B7000GHG Tandil, Argentina

[b]Consejo Nacional de Investigaciones Científicas y Técnicas (CONICET), Av. Rivadavia 1917, C1033AA, Buenos Aires, Argentina

[c]Comisión de Investigaciones Científicas de la Provincia de Buenos Aires (CICPBA), Calle 526 e/10 y 11, B1096APP, La Plata, Argentina

ARTICLE DATA

Article history:
Received 24 December 2011
Received in revised form
2 March 2012
Accepted 6 March 2012

Keywords:
Solidification
Solution treatment
Co–Cr–Mo
Microstructure

ABSTRACT

Three different Co–Cr–Mo–C alloys conforming to ASTM F75 standard were poured in an industrial environment and subjected to a conventional solution treatment at 1225 °C for several time intervals. The microstructural changes and transformations were studied in each case in order to evaluate the way in which treatment time influences the secondary phase fraction and clarify the microstructural changes that could occur. To assess how treatment time affects microstructure, optical microscopy and image analyzer software, scanning electron microscopy and energy dispersion spectrometry analysis were employed.

The main phases detected in the as-cast state were: σ-phase, M_6C, and $M_{23}C_6$ carbides. The latter presented two different morphologies, blocky type and lamellar type. Despite being considered the most detrimental feature to mechanical properties, σ-phase and lamellar carbides dissolution took place in the early stages of solution treatment. $M_{23}C_6$ carbides featured two different behaviors. In the alloy obtained by melting an appropriate quantity of alloyed commercial materials, a decrease in size, spheroidization and transformation into M_6C carbides were simultaneously observed. In the commercial ASTM F75 alloy, in turn, despite being the same phase, only a marked decrease in precipitates size was noticed. These different behaviors could be ascribed to the initial presence of other phases in the alloy obtained from alloyed materials, such as σ-phase and "pearlitic" carbides, or to the initial precipitate size which was much larger in the first than in the commercial ASTM F75 alloy studied. M_6C carbides dissolved directly in the matrix as they could not be detected in samples solution-treated for 15 min.

1. Introduction

Cobalt base alloys (Co–Cr–Mo) are widely used in several medical applications such as knee and hip joint replacement, given their excellent biocompatibility, corrosion and wear resistance, combined with their good mechanical properties [1–4]. They are usually employed in as-cast state conforming to the ASTM F75 standard; and, due to the different chemical composition they may present; their resultant mechanical properties vary significantly. The main defects encountered in the as-cast state are shrinkages, chemical heterogeneity and large grain size [5,6]. The distribution of these inherent defects in the technique employed to obtain the implants explains the low mechanical and fatigue strength values, which can promote the early failure of the device.

* *Corresponding author at:* IFIMAT, Instituto de Física de Materiales Tandil, Pinto 399, B7000GHG, Tandil, Argentina. Tel.: +54 2293 43 9670; fax: +54 2293 43 9679.
E-mail address: jgiacchi@exa.unicen.edu.ar (J.V. Giacchi).

1044-5803/$ – see front matter © 2012 Elsevier Inc. All rights reserved.
doi:10.1016/j.matchar.2012.03.006

With a view to removing casting defects, as-cast Co–Cr–Mo alloys are often subjected to different heat treatments, which are designed to enhance their mechanical properties and prevent fatigue failure. The main thermal treatments applied to these alloys are conventional isothermal solution treatment or homogenization, hot isostatic pressing (hipping) and carbide refining treatments [7].

Several authors have reported that the best elongation values were obtained by hipping treatments [8–11] and carbide refining by melt additions [12]. Notwithstanding this, the most widely used method is solution treatment given the technologies associated to this process and the low cost involved. Even though the data provided by literature regarding temperatures and times applied vary notoriously, this type of treatment is usually performed at temperatures around 1200 °C and for periods ranging from 1 to 4 h.

In conventional solution treatments applied to Co–Cr–Mo alloys, the temperature range available to achieve complete carbide dissolution is very narrow. To achieve the quality demanded by implants used in human beings, the processes require a rigorous control of the variables involved. Treatment temperature is one of said variables, which is determined by the melting point of the interdendritic phases. The values reported in the literature present some discrepancies in this respect too, while the success or failure of the entire process depends on the accuracy of its choice.

Some authors have found that before carbides melting, a solid-state diffusion of the carbide forming elements occurs, while after that, a serrated interface develops [13]. At low treatment temperatures, carbide coarsening, spheroidization [14–16] and incomplete homogenization were observed, also the carbide dissolution kinetics decreased extensively [17]. Treatment temperatures higher than carbides melting point lead to $M_{23}C_6$ carbide fusion [18] and tend to take the system to a thermodynamic equilibrium, since the elements diffusion eliminates the composition gradients [13].

It has been demonstrated that partial carbide dissolution improves not only ductility [8] but also, to a large extent, the alloy fatigue strength in solution-treated samples, [19,20] as it was corroborated by Lorentz et al. [21]. Moreover, it has been reported that short treatments enhance mechanical properties, while prolonged ones result in ductility gain at the expense of other mechanical properties [22,23]. Weeton and Signorelli demonstrated that a solution treatment followed by ageing increases hardness [24]

Clemow and Daniell [17] evaluated the reactions produced during solution treatment and carbide dissolution kinetics. They came to the conclusion that dissolution kinetics was relatively high at the beginning of the cycle and decreased as heat treatment time elapsed. They also concluded that $M_{23}C_6 \rightarrow M_6C$ carbide transformation during high temperature exposure was associated with a decrease in dissolution kinetics. It was further observed that M_6C carbide formation was promoted by an increase in the treatment temperature. On the other hand, Caudillo et al. [22] reported that $M_{23}C_6$ carbides dissolved directly in the matrix without being transformed into an M_6C carbide first.

The microstructure of Co–Cr–Mo alloys in as-cast condition consists in a Co-rich fcc matrix, and precipitates in the interdendritic zones and grain boundary. Such precipitates are mainly formed by $M_{23}C_6$ carbide, the intermetallic phase σ and an eutectic lamellar precipitate, formed by $M_{23}C_6$ carbides and α-fcc phase [18,25]. The precipitation of this pearlitic structure results from the low cooling rate that takes place during solidification [26].

Carbide precipitation represents the major strengthening mechanism in as-cast state for these kinds of alloys, and it is also responsible for low mechanical properties. The type, size and carbide volume fraction depend on the solidification conditions as well as on the chemical composition. The carbide forming elements along with the carbon content present in the alloy play a significant role in the composition and morphology of the precipitated carbides [13]. Even though the effect of the solution treatment on the mechanical properties of the alloy is strongly linked to the carbide features, studies conducted on the characterization of carbides and other phases formed during the solution treatment are really scarce in the literature. In view of the discrepancies evidenced above, a study aiming to elucidate carbide behavior at high temperature during solution treatment is in urgent need.

A previous work [27] accurately studied the microstructure of three different as-cast Co–Cr–Mo alloys and clearly identified the $M_{23}C_6$ and M_6C carbides and σ phase. The aim of this work is to advance our understanding regarding the evolution of the Co–Cr–Mo alloy microstructure during the solution thermal treatment by detecting phases and morphologies present. It also seeks to enlighten their possible transformation at high temperature, evaluating the influence of treatment time.

2. Experimental Procedure

Three different Co–Cr–Mo–C alloys, all of them conforming to ASTM F75 chemical composition specifications, were poured following the methodology adopted and described in a previous work [27]. Sample number one (C1) was obtained by melting an appropriate quantity of alloyed materials of commercial purity. Sample number two (C2) was obtained from the remelted remnant of (C1), checking and adjusting the composition. For this reason it is expected that C2 could have more of metallic inclusions and more inhomogeneities. Sample number three (C3) was obtained by melting commercial material ASTM F75 certified alloy, for comparison purposes. The runs were carried out in an industrial environment, by using a 100 kW induction furnace. The alloys were melted at 1530 °C under an argon atmosphere and then poured into ceramic molds which were preheated to 1200 °C and included a set of three cylinders.

Table 1 introduces the chemical analysis of the resulting alloys, as determined by spark emission spectrometry.

Table 1 – Chemical composition (wt.%) of the studied alloys.

Colada	Co (wt.%)	Cr (wt.%)	Mo (wt.%)	C (wt.%)	W (wt.%)	Si (wt.%)
C1	60.75	30.60	6.14	0.13	0.36	1.29
C2	62.99	28.93	5.83	<0.021	0.38	1.05
C3	64.13	27.01	6.30	<0.021	0.40	1.08
ASTM F75	59.0/ 69.0	27.0/ 30.0	5.0/ 7.0	Max 0.35	Max. 0.2	Max 1.0

The cylinders were cut into slices and then subjected to a solution treatment at 1225 °C and held at this temperature for intervals ranging from 0 to 240 min. Specimens were held at the predetermined temperature for 15, 30, 45, 60, 120 and 240 min, respectively. In all the cases, the samples were quenched in cold water to retain the high temperature microstructure. The samples corresponding to time 0 were the as-cast state specimens for each alloy.

Samples preparation for optical and scanning electron microscopy was carried out with conventional procedures for polishing, from 600 grid Si-C paper until a 0.05 μm alumina suspension. The specimens were thoroughly cleaned to remove any polishing remnant. To reveal the microstructure and study the precipitates evolution, a two-stage etching was used, selecting a combination of etchants that, in a first stage, revealed the dendritic matrix features with a light electrolytic chromic acid etchant and then stained the second phases for their identification [28].

Optical microscopy was used for a first identification of secondary phases, and image analysis, together with carbide fraction quantification, was performed using Image Pro Plus™ software. To provide a more accurate characterization, the samples were examined by scanning electron microscopy (SE-SEM) with a JEOL JSM-6460LV microscope, and energy dispersive spectroscopy (EDS) techniques were employed, even though the EDS technique provides a semi-quantitative analysis. The system used was an EDAX Genesis XM4-Sys 60, equipped with a multichannel analyzer EDAX mod EDAM IV, Sapphire Si(Li) detector and a super ultra thin beryllium window, with a 20 kV acceleration voltage.

3. Results and Discussion

The microstructure of all the samples studied in as-cast condition and observed by optical microscopy was mainly formed by dendritic α-fcc Co-rich grains and carbides precipitated in grain boundaries (GBs) and interdendritic spaces [27]. Despite the fact that precipitates feature a wide chemical carbide composition range, they were well identified by the color obtained using the etching technique and the EDS analysis.

3.1. *Sample C1*

The main precipitates were identified by color metallography and EDS analysis as σ phase, $M_{23}C_6$ and coarse lamellar phase, in agreement with reports in the literature [29]. Fig. 1 details the as-cast microstructure in an optical micrograph, while Fig. 2 illustrates a secondary electron SEM image with the main phases marked. The EDS analysis of the "pearlitic" phase revealed that it was formed by thin interlayed plates of $M_{23}C_6$ carbides and α-fcc phase, in accordance with Kilner [18] and Hëro [30]. Fig. 3a and b depicts the EDS analysis for the carbide and σ tetragonal phase.

During the solution treatment evolution, the initial "pearlitic" colonies and σ phase dissolved in the first 15 min, and their presence could not be detected in any solution-treated sample under longer term treatment. This could be expected given the fact that the "lamellar" structure permits a faster diffusion of the carbide forming elements in the α-matrix

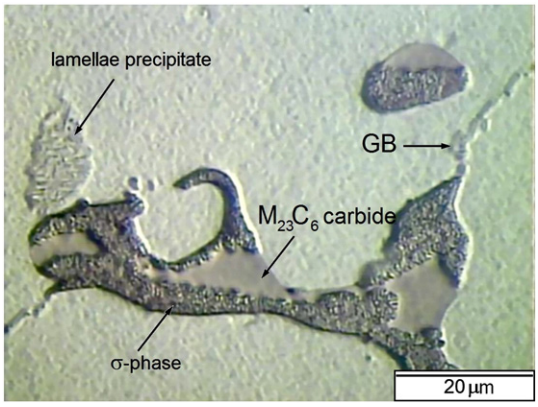

Fig. 1 – Optical micrograph of the main phases in as-cast state, detected in C1 alloy by color metallography.

and therefore blocky type carbides dissolve more slowly than lamellar carbides do.

As the solution treatment progresses, the $M_{23}C_6$ carbide suffers a spheroidization and transforms according to the $M_{23}C_6 \rightarrow M_6C$ reaction, as it can be noticed in Figs. 4 and 5, respectively. Such transformation was corroborated by the EDS analysis and consistent with Clemow and Daniell [17], Lane [30] and Mancha et al. [13] who established that carbide decomposition takes place through a solid state reaction. The EDS analysis corresponding to the $M_{23}C_6$ and M_6C carbides are shown in Fig. 6a and b, respectively. Fig. 7 demonstrates that in samples from C1 solution-treated for 45 min, recrystallization also occurs as a secondary effect. A decrease in carbide size, concomitant with the transformation, could be observed as well.

3.2. *Sample C2*

The coexistence of two different types of carbides was found in as-cast condition in this alloy, probably owing to a change in the cooling rate. Fig. 8 depicts the carbides identified by color metallography as $M_{23}C_6$ and M_6C needle-type. Fig. 9a and b, in turn, shows EDS analysis results. The latter carbide (M_6C) was only detected in the as-cast state, so it could be assumed that this carbide dissolved directly in the matrix

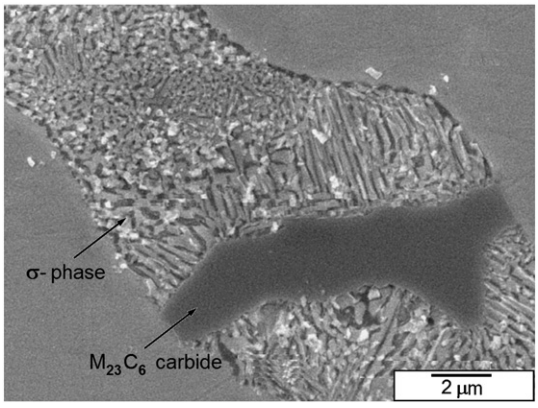

Fig. 2 – SEM micrograph of C1 alloy with main precipitates marked.

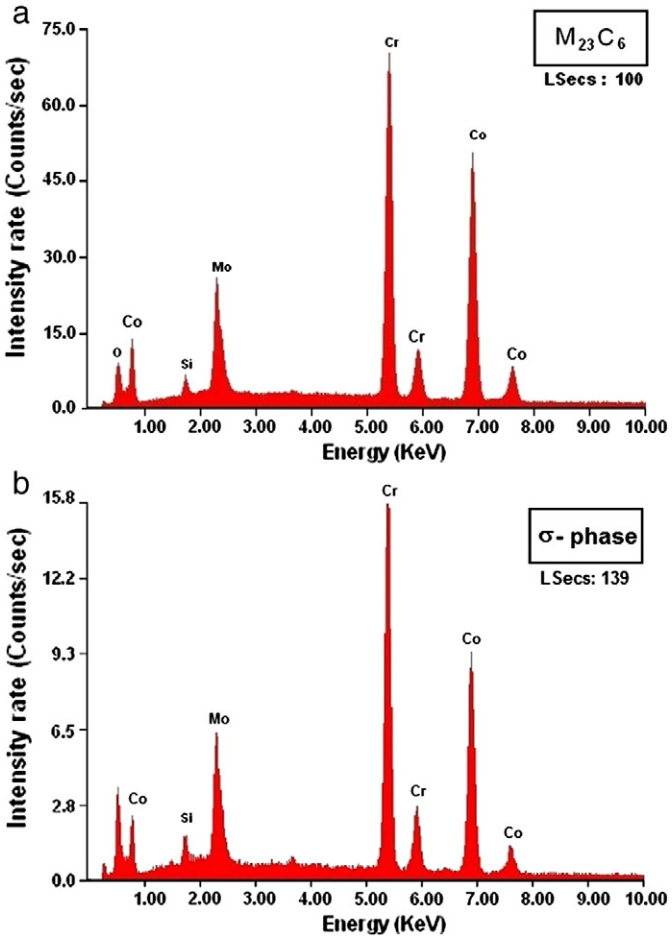

Fig. 3 – EDS analysis of a) $M_{23}C_6$ carbide detected in as-cast C1 alloy b) σ-phase present in as-cast C1 alloy.

exhibiting no transformation. In regard to the $M_{23}C_6$ carbide present in C2, despite being the same phase identified in C1, its behavior differed completely, as no transformation was noticed. A decrease in $M_{23}C_6$ carbides size was detected instead, indicating that, in this case, this phase dissolved directly in the matrix.

3.3. *Sample C3*

Only $M_{23}C_6$ carbides were identified in this alloy in as-cast samples, as illustrated in Figs. 10 and 11. Carbides present in solution-treated specimens from C3 alloy behaved analogously to C2 alloy. The prolonged exposure to high temperature

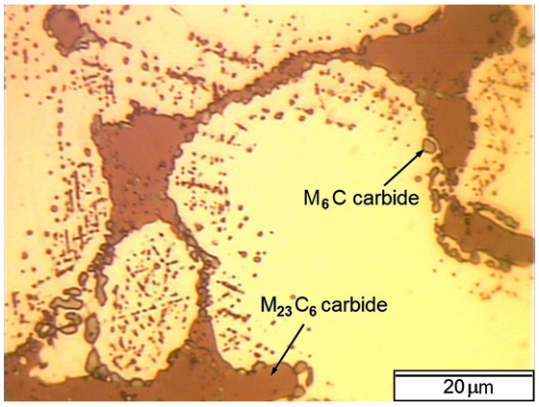

Fig. 4 – Optical micrograph showing microstructural evolution in C1 alloy. Sample solution-treated for 15 min with main phases identified as $M_{23}C_6$ and M_6C carbides.

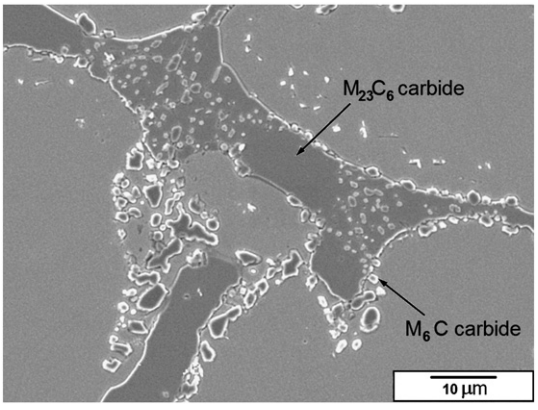

Fig. 5 – SE-SEM image showing spheroidization and $M_{23}C_6 \rightarrow M_6C$ transformation in C1 alloy. Sample corresponds to 1 h of solution treatment.

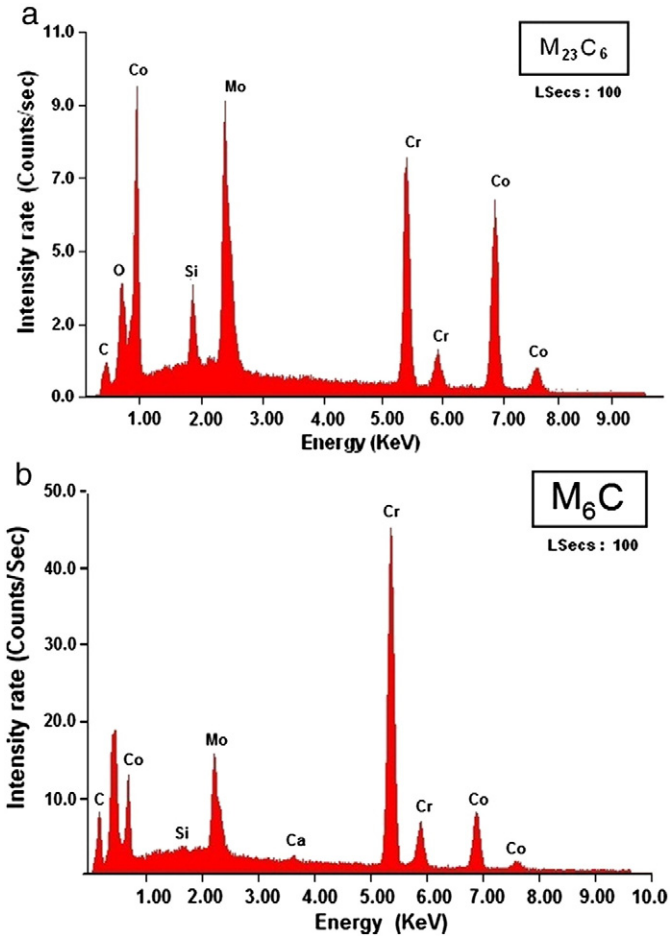

Fig. 6 – EDS analysis corresponding to the main phases found in C1 after 1 h of treatment a) $M_{23}C_6$ carbide and b) M_6C, respectively.

dissolved most carbides, and those remaining featured such a small size that it hindered their visualization by optical microscopy. Fig. 12 is a secondary electron SEM image of a 120 minute solution-treated specimen. The EDS analysis shown in Fig. 13 indicates that it is a $M_{23}C_6$ carbide.

3.4. *Variation of Carbide Content*

The variation of the carbide content with increasing solution treatment time was studied for each alloy. Each quantitative determination of carbide content was made at 100× magnification

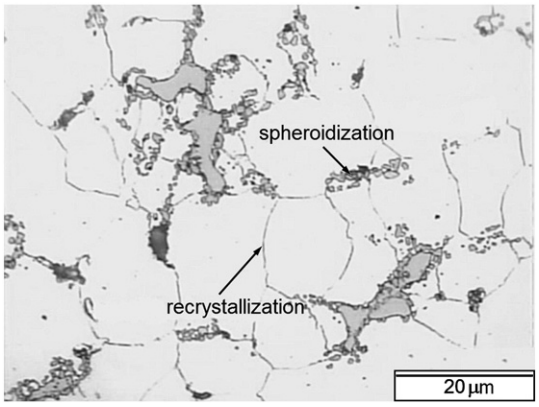

Fig. 7 – OM where recrystallization and $M_{23}C_6$ carbide decomposition can be observed. Sample from C1 solution-treated for 45 min.

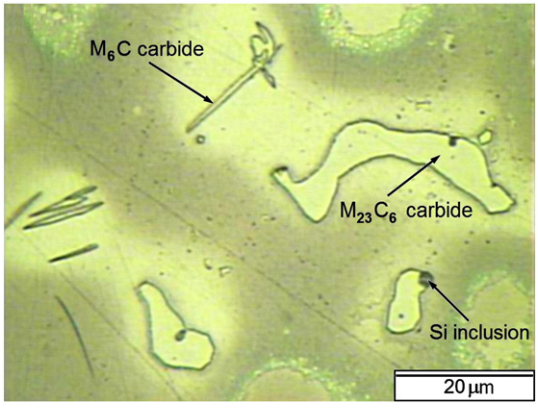

Fig. 8 – OM of as-cast C2 alloy showing $M_{23}C_6$ and M_6C carbides in coexistence. Phases detected by color metallography.

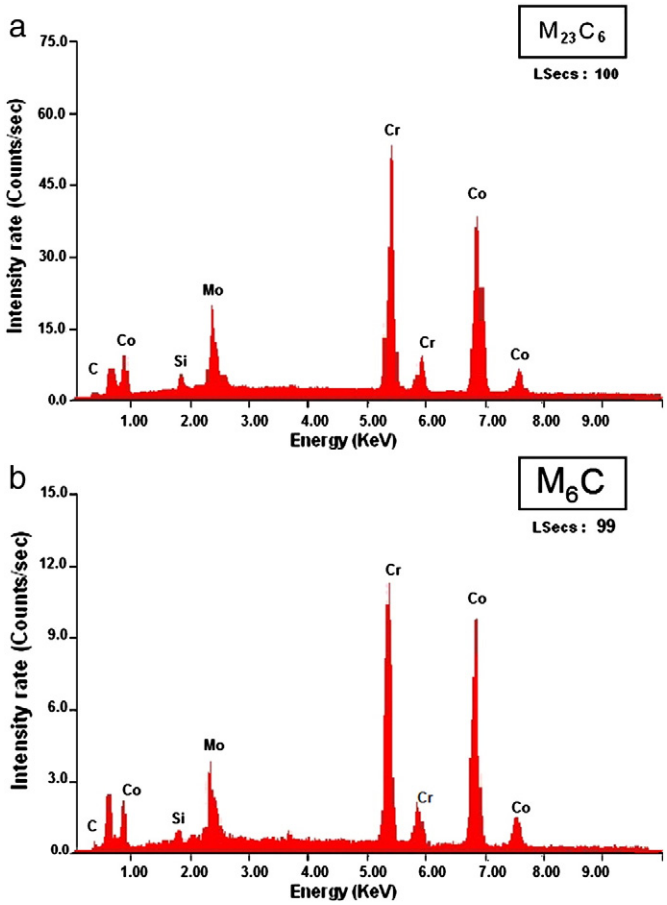

Fig. 9 – EDS analysis of the present phases in as-cast C2 alloy a) $M_{23}C_6$ carbide phase and b) M_6C carbide phase.

on 20 fields and the data obtained were processed by image analyzer software. For the three alloys under study, the carbide fraction decreased significantly in short treatments, whereas in times ranging from 120 to 240 min, variation was slight. The solution treatment promotes a pronounced decrease in the size of secondary phases for the first 90 min. Since the initial carbide size difference between the alloys was very large, the data presented in Fig. 14 were normalized. Initial carbide sizes were 262, 127 and 45 μm in average for C1, C2 and C3 as-cast samples, respectively. Therefore the carbide variation with the solution time is reported based on the percentage of size decrease.

Carbide size reduction reached 62%, nearly 71% and 97% for samples solution-treated for 240 min from C1, C2 and C3 alloys, respectively, as illustrated in Fig. 14.

It is noteworthy that as the solution treatment time increased, a high temperature oxide layer was formed in heat

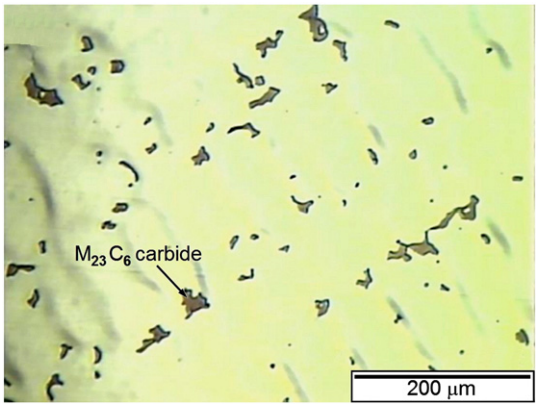

Fig. 10 – OM with main colored phases detected in C3 alloy. $M_{23}C_6$ carbides with extremely homogeneous distribution were identified.

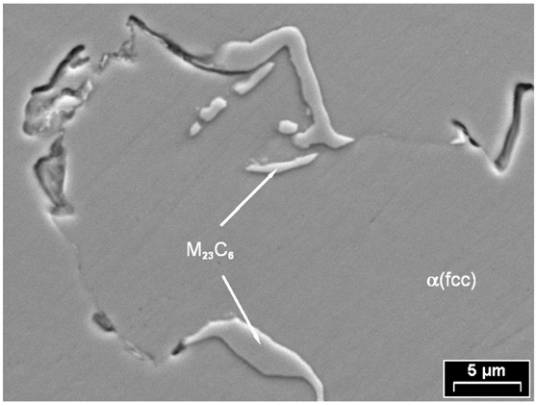

Fig. 11 – Electron micrograph with main detected phases in C3 alloy.

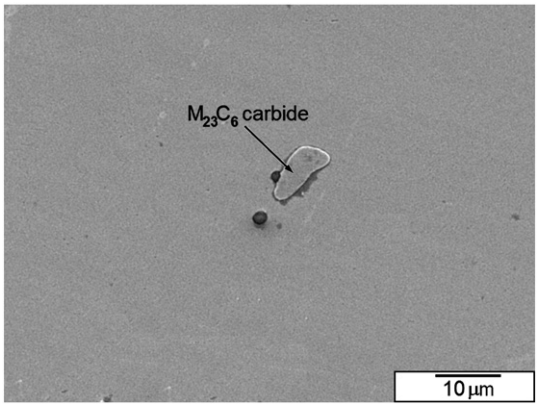

Fig. 12 – Main phases present in C3 alloy after 120 min of solution treatment, shown in an electron micrograph (SE-SEM).

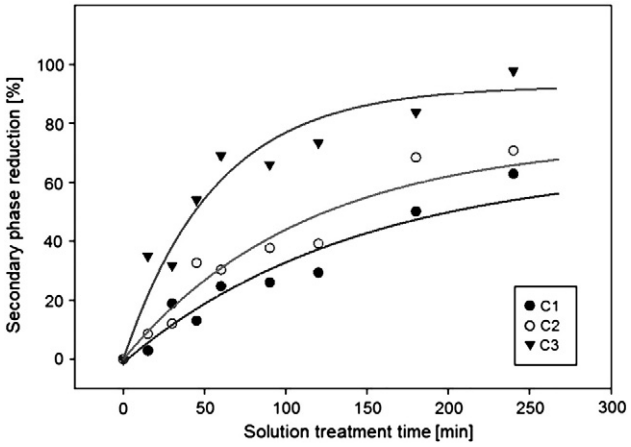

Fig. 14 – Evolution of carbide content (percentage of reduction) as a function of treatment time for the alloys under study.

C2. Its thickness increased as treatment time did, up to reaching 1 mm thickness in the 240 minute solution-treated specimen. The oxide layer analysis applying EDS technique revealed that it was an oxide formed by the main alloying elements. The oxide film SEM image and the EDS analysis corresponding to the oxide layer are shown in Figs. 15 and 16, respectively.

The formation of this oxide layer cannot be tolerated in the manufacture of biocompatible devices; since oxide microparticles could be retained in ulterior sterilization processes and change the device properties. It could even be released in the human body as wear or corrosion products. Despite the fact that the chemical composition of the alloys studied does not vary significantly, indeed there is an element that, given its distribution or size, becomes the catalyst in the formation of this chromium rich layer. Further investigations should be conducted to clarify the formation mechanism of this layer.

4. Conclusions

Three Co–Cr–Mo–C alloys poured in an industrial environment were solution treated at 1225 °C for several time intervals. The microstructural changes and transformations were studied in each case. According to the results obtained, the following conclusions can be drawn:

- The optical, SEM microscopy and EDS analysis, showed that the phases present in the as-cast state were well identified as σ-phase, M_6C and $M_{23}C_6$ carbide, respectively. The latter presented two different morphologies, blocky type and lamellar type. Despite being mentioned as the most detrimental feature to the mechanical properties, σ-phase dissolution takes place in the first minutes of solution treatment.
- With respect to $M_{23}C_6$ carbides, two different behaviors were observed. In C1 alloy, a decrease in size, spheroidization and transformation into M_6C carbides were simultaneously appreciated. In C3 alloy, despite being the same phase, only a marked decrease in the size of the precipitates was noticed. These different behaviors could be ascribed to the initial presence of other phases in C1 such as σ-phase and "pearlitic" carbides, which, once dissolved in the early stages of treatment, may have increased the transition element rates in the matrix facilitating transformation; or due to the initial precipitate size which was much larger in C1 than in the other two alloys under study.

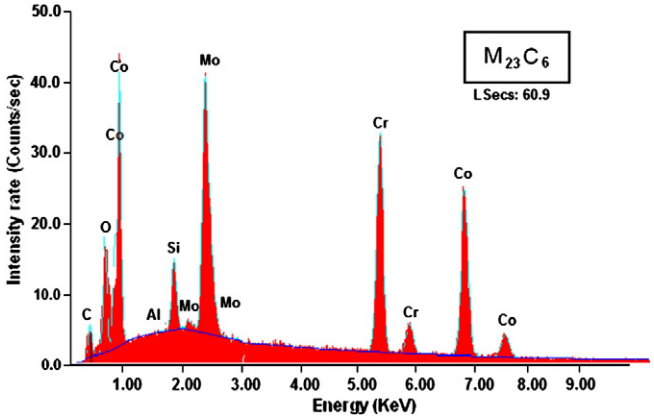

Fig. 13 – EDS analysis of the $M_{23}C_6$ carbide phase detected in C3 commercial alloy.

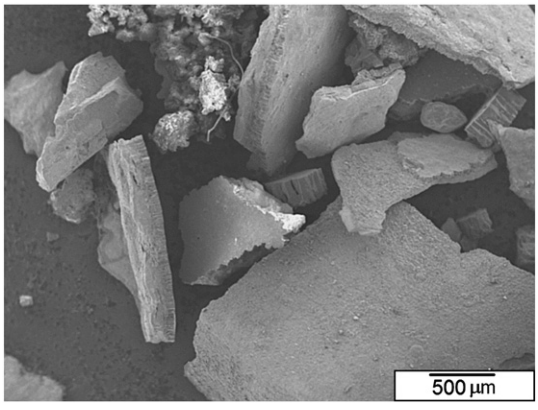

Fig. 15 – SE-SEM image of the oxide layer formed at high temperature in C2 alloy.

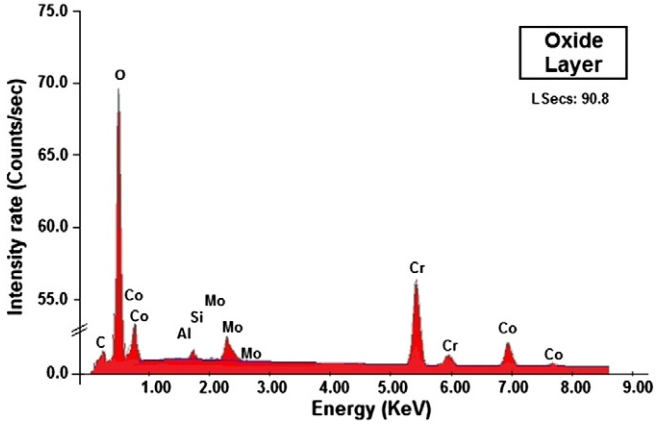

Fig. 16 – EDS analysis of the oxide layer formed in C2, which resulted in chromium-rich oxide.

- Specimens from C3 alloy showed precipitates with an initial, much smaller size and with a more homogeneous distribution in the interdendritic space of the as-cast structure with respect to the other two alloys studied. These phases could be identified only with large magnifications, which were achieved by SEM microscopy. As a consequence, shorter times were needed to dissolve most carbides.
- The decrease in carbides size turned out to be 62%, about 71% and 97% for C1, C2 and C3 alloys, respectively, for samples solution-treated for 240 min.
- Finally, samples from C2 alloy generated an oxide layer around the solution-treated samples. This oxide film was mainly formed by chromium. The anomalous behavior of this particular alloy, which was obtained by remelting C1 alloy, could be caused by carbide distribution during casting and by the high level of Si-metallic inclusions detected in the as-cast evaluation.

Acknowledgments

This work was carried out at IFIMAT, and partially supported by ANPCyT, CONICET, SECAT-UNCPBA and CICPBA.

REFERENCES

[1] Zhuang L, Langer EW. Effects of alloy additions on the microstructure and tensile properties of cast Co–Cr–Mo alloy used for surgical implants. J Mater Sci 1989;24:4324–30, doi:10.1007/BF00544506.
[2] Lee SH, Takahashi E, Nomura N, Chiba A. Effect of carbon addition on microstructure and mechanical properties of wrought Co–Cr–Mo implant alloy. Mater Trans 2006;47:287–90, doi:10.2320/matertrans.47.287.
[3] Lee SH, Nomura N, Chiba A. Effect of Fe addition on microstructures and mechanical properties of Ni- and C-free Co–Cr–Mo alloys. Mater Trans 2007;48:2207–11, doi:10.2320/matertrans.MRA2007004.
[4] Lee S, Nomura N, Chiba A. Significant improvement in mechanical properties of biomedical Co–Cr–Mo alloys with combination of N addition and Cr enrichment. Mater Trans 2008;49:260–4, doi:10.2320/matertrans.MRA2007220.
[5] Campbell J. Castings: the new metallurgy of cast metals. 2nd edition. Oxford, UK: Elsevier; 2004.
[6] Stefanescu DM. Science and engineering of casting solidification. 2nd edition. USA: Springer; 2009.
[7] Kurosu S, Matsumoto H, Chiba A. Grain refinement of biomedical Co–27Cr–5Mo–0.16N alloy by reverse transformation. Mater Lett 2010;64:49–52, doi:10.1016/j.matlet.2009.10.001.
[8] Hollander R, Wulff J. New technology for mechanical property improvement of cast Co–Cr–Mo–C surgical implants. J Biomed Mater Res 1975;9:367–9, doi:10.1002/jbm.820090311.
[9] Opris CD, Liu R, Yao MX, Wu XJ. Development of Stellite alloy composites with sintering/HIPping technique for wear resistant applications. Mater Des 2006;37A:3197–203, doi:10.1016/j.matdes.2005.08.004.
[10] Amigo Borrás V, Vicente A, Romero F, Paolini A. Influencia del tratamiento HIP en la distribución de los carburos en prótesis CoCrMo. Bol Soc Esp Ceram Vidrio 2004;43:573–7, doi:10.3989/cyv.2004.v43.i2.597.
[11] Coke JR. Heat treatment of cast Co–Cr–Mo–C surgical implant alloy. Thesis to achieve Master of Science Degree MIT, 1975.
[12] Kilner T, Dempsey AJ, Pilliar RM, Weatherly GC. The effects of nitrogen addition to a cobalt–chromium surgical implant alloy. J Mater Sci 1987;22:565–74, doi:10.1007/BF01160770.
[13] Mancha H, Carranza E, Escalante JI, Mendoza G, Méndez M, Cepeda F, et al. $M_{23}C_6$ carbide dissolution mechanisms during heat treatment of ASTM F-75 implant alloys. Metall Mater Trans A 2001;32:979–84, doi:10.1007/s11661-001-0355-8.
[14] Shtansky DV, Nakai K, Ohmori Y. Crystallography and interface boundary structure of pearlite with M_7C_3 carbide lamellae. Acta Mater 1999;47:1105–15, doi:10.1016/S1359-6454(99)00011-7.
[15] García C, Caruana G, Alvarez LF. Control of $M_{23}C_6$ carbides in 0.45C-13Cr martensitic stainless steel by means of three representative heat treatment parameters. Mater Sci Eng A Struct 1998;241:211–5, doi:10.1016/s0921-5093(97)00491-7.
[16] García C, Alvarez LF, López V, Jiménez JA. Effects of carbide forming elements on the response to thermal treatment of the X45Cr13 martensitic stainless steel. J Mater Sci 1998;33:4095–100, doi:10.1023/A:1004424329556.
[17] Clemow AJ, Daniell BL. Solution treatment behavior of Co–Cr–Mo alloy. J Biomed Mater Res 1979;13:265–79, doi:10.1002/jbm.820130208.
[18] Kilner T, Pilliar RM, Weatherly GC, Allibert C. Phase identification and incipient melting in a cast Co–Cr surgical implant alloy. J Biomed Mater Res 1982;16:63–79, doi:10.1002/jbm.820160109.
[19] Cohen J, Rose RM, Wulff J. Recommended heat treatment and alloy additions for cast Co–Cr surgical implants. J Biomed Mater Res 1978;12:935–7, doi:10.1002/jbm.820120613.

[20] Dobbs HS, Robertson JLM. Heat treatment of cast Co–Cr–Mo for orthopaedic implant use. J Mater Sci 1983;18:391–401, doi: 10.1007/BF00560627.
[21] Lorentz M, Semlitsch M, Panic B, Weber H, Willert HG. Fatigue strength of cobalt-base alloys with high corrosion resistance for artificial hip joints. Eng Med 1978;7:241–50, doi: 10.1234/EMED_JOUR_1978_007_061_02.
[22] Caudillo M, Herrera Trejo M, Castro M, Ramírez E, González C, Juárez J. On carbide dissolution in an as-cast ASTM F-75 alloy. J Biomed Mater Res 2002;59:378–85, doi:10.1002/jbm.10001.
[23] Herrera M, Espinoza A, Méndez J, Castro M, López J, Rendón J. Effect of C content on the mechanical properties of solution treated as-cast ASTM F75 alloys. J Mater Sci Mater Med 2005;16:607–11, doi:10.1007/S10856-005-2530-8.
[24] Weeton JW, Signorelli RA. Structures, micro-constituents and hardness of a wrought cobalt base alloy. Trans Am Soc Met 1955;47:815–52.
[25] Weeton JW, Signorelli RA. An investigation of lamellar structures and minor phases in eleven cobalt base alloys before and after heat treatment, 3109. NACA Technical Note; 1954.
[26] Ramírez-Vidaurri LE, Castro-Román M, Herrera-Trejo M, García-López CV, Almanza-Casas E. Cooling rate and carbon content effect on the fraction of secondary phases precipitate in as-cast microstructure of ASTM F-75 alloy. J Mater Process Technol 2009;209:1681–7, doi:10.1016/j.jmatprotec.2008.04.039.
[27] Giacchi JV, Morando CN, Fornaro O, Palacio H. Microstructural characterization of as-cast biocompatible Co–Cr–Mo alloys. Mater Charact 2011;62:53–61, doi:10.1016/j.matchar.2010.10.011.
[28] Ramírez L, Castro M, Méndez M, Lacaze J, Herrera M, Lesoult G. Precipitation path of secondary phases during solidification of the CoCrMoC alloy. Scr Mater 2002;47:811–6, doi:10.1016/S1359-6462(02)00305-6.
[29] Vander Voort G. ASM Metals Handbook Vol. 9 — metallography and microstructures. 4th edition. USA: ASM; 2004.
[30] Lane JR, Grant NJ. Carbide reactions in high temperature alloys. Trans Am Soc Met 1952;44:113–37.